

Accurate Scene Text Recognition with Efficient Model Scaling and Cloze Self-Distillation

Andrea Maracani^{1*} Savas Ozkan^{1†} Sijun Cho² Hyowon Kim² Eunchung Noh²
 Jeongwon Min² Cho Jung Min² Dookun Park² Mete Ozay¹
¹Samsung R&D Institute UK ²Samsung Electronics

Abstract

Scaling architectures have been proven effective for improving Scene Text Recognition (STR), but the individual contribution of vision encoder and text decoder scaling remain under-explored. In this work, we present an in-depth empirical analysis and demonstrate that, contrary to previous observations, scaling the decoder yields significant performance gains, always exceeding those achieved by encoder scaling alone. We also identify label noise as a key challenge in STR, particularly in real-world data, which can limit the effectiveness of STR models. To address this, we propose Cloze Self-Distillation (CSD), a method that mitigates label noise by distilling a student model from context-aware soft predictions and pseudolabels generated by a teacher model. Additionally, we enhance the decoder architecture by introducing differential cross-attention for STR. Our methodology achieves state-of-the-art performance on 10 out of 11 benchmarks using only real data, while significantly reducing the parameter size and computational costs.

1. Introduction

Scene Text Recognition (STR) aims to automatically transcribe text in natural scenes, enabling applications in autonomous driving [51], augmented reality [27], language translation [43], and assistive technologies. Unlike traditional Optical Character Recognition (OCR), which typically works with clean or scanned documents, STR faces unique challenges due to the diverse and uncontrolled nature of text in real-world environments. In particular, text in these settings can vary significantly in orientation, font style, shape, size, color, formatting, and aspect ratio. It often appears on complex backgrounds that may also include reflections, transparency, or occlusions. Furthermore, images might have poor quality, suffering from issues such as blurring, low resolution, and noise [23].

Recent research has led to notable performance improve-

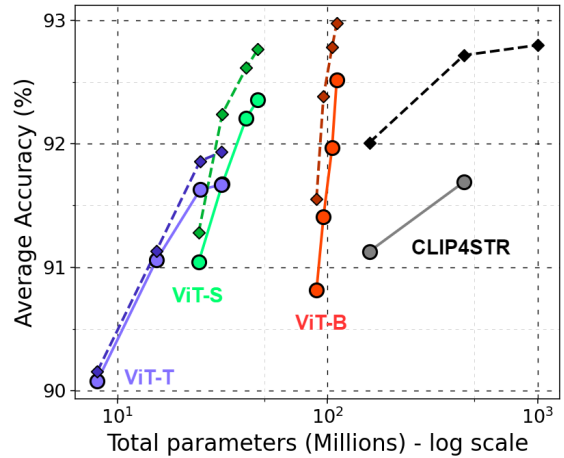


Figure 1. **Average word accuracy (%)** on 11 STR benchmarks for the models with ViT-T, ViT-S and ViT-B vision encoders and 4 different decoder sizes (see Sec. 4.1). Results are compared with the previous state-of-the-art model, CLIP4STR [54]. Results using **Real** training dataset (3.3M images) are depicted with solid lines and circle markers, while results using **RBU** training dataset (6.5M images) are shown with dashed lines and diamond markers. The x-axis represents the **total number of model parameters** (in millions) on a logarithmic scale.

ments in STR by enhancing training methods [15], deploying novel architectures [1, 54], and exploring the effects of model scaling [31]. Despite these advancements, current STR models still face important challenges that limit their effectiveness. Our work is motivated by the following research question:

What are the primary bottlenecks currently limiting STR, and what strategies can be employed to improve both accuracy and efficiency?

Throughout our analysis, we identify three important limitations: **(i)** sub-optimal model scaling, **(ii)** noisy labels in training data, and **(iii)** architectural limitations within current model designs.

Sub-optimal model scaling. Prior scaling analyses [31] have explored scaling laws for STR, demonstrating that

*Main Authorship. a.maracani@samsung.com

†Senior Authorship

increasing model size and data volume can lead to performance gains, following scaling trends similar to those observed in Natural Language Processing [16]. In particular, the CLIP4STR [54] methodology, which leverages CLIP [30] pre-training and integrates a cross-modal correction branch, achieves the best results at scale among all considered methods. However, [31] also found that increasing the decoder depth in PARSeq [3] results in decreased performance, leading to an emphasis on encoder scaling.

In this work, we provide an in-depth analysis of the effects of independently scaling the encoder and decoder components under different data volumes. Contrary to previous findings, we demonstrate that decoder scaling is indeed essential for achieving optimal STR performance.

As illustrated in Fig. 1, increasing the decoder size provides substantial benefits for any visual encoder and results in more favorable scaling laws. Notably, proper model scaling alone is sufficient to surpass (on average) previous state-of-the-art performance without the need for CLIP pre-training or additional cross-modal branches. Furthermore, this approach substantially reduces the number of parameters and FLOPs.

Noisy labels in training data. Our analysis indicates that, under some conditions, scaling the vision encoder may lead to diminishing returns or a decrease in accuracy, especially when STR models are trained on limited real data. In this context, we observe that text annotations of STR datasets often suffer from inconsistencies, errors and noise, which can negatively impact STR performance (Fig. 2). To address this issue, we propose a novel *Cloze Self-Distillation* (CSD) technique. In CSD, a model serving as a teacher, is first trained and used to generate predictions on training data. These predictions are then refined using a cloze-filling approach: each character is re-predicted using all other characters as textual context, resulting in more accurate, informative and context-aware soft predictions. We then distill the teacher into an identical student model on the same training set by employing the teacher’s hard predictions as ground truth and a knowledge distillation term [14] that minimizes the divergence between the student’s limited-context predictions (obtained through permuted language modeling [49]) and the teacher’s full-context cloze predictions. This technique enables the student to update its parameters with the richer, context-aware outputs of the teacher, while operating under the constraints of limited context. We provide empirical evidence demonstrating the effectiveness of CSD in mitigating label noise and inconsistencies, leading to substantial performance improvements.

Architectural limitations. We extend our analysis on the decoder of our STR model by introducing additional architectural improvements. Inspired by Differential Transformer [50], we propose a novel Differential Permutation Language Decoder that employs Differential Cross-

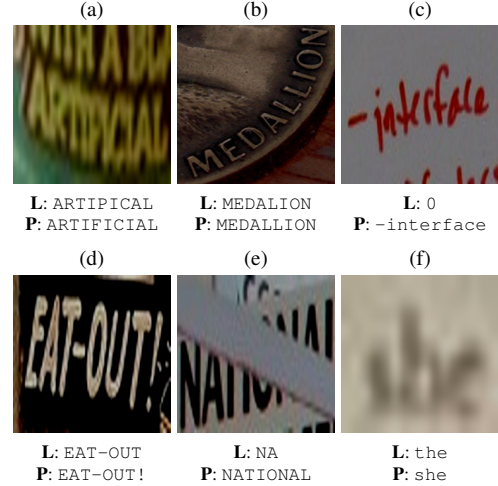


Figure 2. **Examples of label inconsistencies and errors in the training set.** For each image, we show the ground truth label (L) and the teacher-generated pseudolabel (P). Subfigures (a-c) illustrate typical label errors, such as spelling mistakes or missing characters. Subfigures (d,e) highlight label inconsistencies, where punctuation or occluded parts are not annotated. Subfigure (f) demonstrates a labelling error caused by severe degradation in the image quality.

attention layers and SwiGLU activations [33], addressing the limitation of previous architecture in focusing on relevant context.

Our contributions can be summarized as follows:

- **A detailed analysis of encoder-decoder scaling** for STR (Sec. 4.1), demonstrating substantial performance improvements with decoder-focused scaling, contrary to findings in previous studies.
- **Cloze Self-Distillation (CSD)** technique that addresses label noise by leveraging context-rich cloze predictions (Sec. 4.2), improving the robustness and performance of models across different data regimes.
- **An enhanced decoder architecture** that incorporates Differential Cross-Attention and SwiGLU activations (Sec. 4.3), achieving further improvements in STR performance.

Through extensive empirical evaluation (Sec. 5.6), we demonstrate that the our enhanced decoder architecture and CSD, together with proper model scaling, consistently outperform previous approaches. Specifically, **our STR method achieves the state-of-the-art performance on 10 out of 11 benchmarks**, with substantial reductions in parameter size and computational costs (FLOPs).

2. Related work

Scene Text Recognition. A branch of STR approaches relies on Connectionist Temporal Classification (CTC) [12]. These include approaches such as CRNN [35], DTRN [13] and Star-Net [22], that utilize Convolutional Neural Net-

works (CNNs) and Recurrent Neural Networks (RNNs), as well as Rosetta [5]. They utilize the character interactions using convolutions and recurrent structures. All these methods are trained with the CTC loss which enables to predict variable-length sequences without requiring explicit alignment. Another direction of approaches integrates attention mechanisms, as seen in RARE [36], R2AM [20], ASTER [38] and DAN [46], to capture the complex spatial dependencies of text characters. Similarly, VITSTR [1] uses an encoder-only Vision Transformer [9] to encode the image patches that are directly classified into characters. A limitation of these approaches is that language modelling is not incorporated, resulting in a weakness to strong perturbations and occlusions commonly encountered in STR. To address this issue, a subsequent amount of methods incorporates context-aware mechanisms by integrating external or internal architectures, such as NRTR [34], ABINet [10], TrOCR [21], and PARSeq [3]. In particular, PARSeq proposes to utilize an encoder-decoder transformer architecture and to train the model with an end-to-end scheme with permuted language modeling [49]. Similarly, DTrOCR [11] uses a decoder-only transformer (GPT-2 model [29]) to directly decode image patches. Exploiting a pre-training on a large-scale simulated dataset and a fine-tuning step on real data, this method demonstrates state-of-the-art performance in many STR benchmarks.

Empirical analyses. Baek et al. [2] examine the impact of training datasets on performance and inconsistencies in evaluation in the field of STR. Recently, Rang et al. [31] investigate how model size, data volume, and computational resources affect the STR performance, revealing smooth power-law relationships between these factors and model accuracy.

Knowledge distillation (KD) [14] is a technique to enhance the model efficiency by replicating the knowledge of a complex *teacher* model into a smaller *student* model. In the context of STR, [4] employs KD to unify STR and Handwriting Text Recognition models, while [48] explore a symmetrical distillation strategy to capture the visual and linguistic knowledge of CLIP.

3. Setup

Notation. We denote an input image as $\mathbf{x} \in \mathcal{X}$, where \mathcal{X} is the image space, and a sequence of characters as $\mathbf{y} = [y_1, y_2, \dots, y_L] \in \mathcal{Y}$, where \mathcal{Y} is the sequence space, L is the sequence length and $(\forall i) y_i$ belongs to a fixed vocabulary \mathcal{C} (character set). We use $\mathbf{y}_{<t} = [y_1, y_2, \dots, y_{t-1}]$ to denote the subsequence of \mathbf{y} previous to position t and $\mathbf{y}_{\neq t} = [y_1, \dots, y_{t-1}, y_{t+1}, \dots, y_L]$ to denote the sequence \mathbf{y} excluding the character in position t . In our mathematical formulation, we consider all sequences to be of the same length L . This can be achieved by right-padding shorter sequences with a special token $[\text{PAD}] \in \mathcal{C}$. We use $\sigma(\cdot)$ to

denote the softmax function and $D_{\text{KL}}(p||q)$ to denote the Kullback-Leiber divergence between distributions p and q .

Problem Formulation. We formulate the STR problem as an image-conditioned generative language modeling task, where the objective is to model the conditional probability of a target characters sequence \mathbf{y} given the input image \mathbf{x} . Let \mathcal{D} represent the underlying data distribution over $\mathcal{X} \times \mathcal{Y}$ and let $p_\theta(\mathbf{y}|\mathbf{x})$ denote the probabilistic model, parametrized by θ . The goal is to minimize the negative log-likelihood (NLL) of the sequence \mathbf{y} given \mathbf{x} , formulated by:

$$\min_{\theta} \mathbb{E}_{(\mathbf{x}, \mathbf{y}) \sim \mathcal{D}} [-\log p_\theta(\mathbf{y}|\mathbf{x})] \quad (1)$$

Since we do not have direct access to real data distribution \mathcal{D} , we approximate the objective using a finite dataset of i.i.d. samples $\{(\mathbf{x}_i, \mathbf{y}_i)\}_{i=1}^n \sim \mathcal{D}^n$, yielding:

$$\min_{\theta} \frac{1}{n} \sum_{i=1}^n -\log p_\theta(\mathbf{y}_i|\mathbf{x}_i) \quad (2)$$

In standard language modeling, the model computes the full probability of the sequence \mathbf{y} by conditioning each character y_t on the previous sub-sequence $\mathbf{y}_{<t}$ that can be represented by:

$$p_\theta(\mathbf{y}|\mathbf{x}) = \prod_{t=1}^L p_\theta(y_t|\mathbf{y}_{<t}, \mathbf{x}) \quad (3)$$

This factorization enables the model to capture the left-to-right sequential dependencies of \mathbf{y} . During inference an output sequence $\hat{\mathbf{y}}$ can be predicted by iteratively selecting the most likely character c over the character set \mathcal{C} . For each position $t \in [1, L]$, it can be formulated by:

$$\hat{y}_t = \arg \max_{c \in \mathcal{C}} p_\theta(y_t = c|\hat{\mathbf{y}}_{<t}, \mathbf{x}) \quad (4)$$

Permutation Language Modeling (PLM). Initially introduced by [49] to enable bidirectional context utilization in language models, PLM has been extended to the domain of STR by PARSeq [3], to provide a flexible modeling approach. PLM generalizes the factorization of Eq. 3 by considering multiple possible orders of character generation. Let Π denote the set of all possible permutations of character indices $[1, 2, \dots, L]$ for a sequence of length L . Then, the factorization based on the order induced by the permutation $\pi \in \Pi$ is:

$$p_\theta(\mathbf{y}|\mathbf{x}) = \prod_{t=1}^L p_\theta(y_{\pi_t}|\mathbf{y}_{\pi_{<t}}, \mathbf{x}) \quad (5)$$

By introducing this factorization in the NLL minimization problem of Eq. 1, the PLM objective becomes:

$$\min_{\theta} \mathbb{E}_{(\mathbf{x}, \mathbf{y}) \sim \mathcal{D}} \left[\sum_{\pi \in \Pi} -\log p_\theta(y_{\pi_t}|\mathbf{y}_{\pi_{<t}}, \mathbf{x}) \right] \quad (6)$$

The empirical PLM counterpart of Eq. 2 can be easily derived using this equation. By removing the left-to-right constraint, PLM enables the model to use bidirectional information during training, enhancing its ability to handle diverse text layouts and ultimately improves the accuracy in STR [3]. In our model, we employ PLM in all experiments. **Cloze-filling refinement.** After PLM training, the model p_θ can be used to infer the sequences in any order, enabling the application of *Cloze-filling refinement*. In this approach, first an initial prediction \hat{y} is made for an image \mathbf{x} , usually using the standard left-to-right decoding (Eq. 4). Later, each position t in the sequence is re-predicted, given all the other characters $\hat{y}_{\neq t}$ in order to obtain the the cloze-refined prediction \hat{y}_t^{cloze} formulated by:

$$\hat{y}_t^{\text{cloze}} = \arg \max_{c \in \mathcal{C}} p_\theta(y_t = c | \hat{y}_{\neq t}, \mathbf{x}) \quad (7)$$

4. Methodology

In this work, we consider a STR model p_θ composed by an image encoder E and a text decoder D . Given an input image \mathbf{x} , the encoder E computes a sequence of vision tokens that constitute the latent representations $\mathbf{z} \in \mathcal{Z}$. Later, for a random permutation π and given \mathbf{z} , a sequence position π_t and previous characters $\mathbf{y}_{\pi_{<t}}$, the decoder D estimates the logits over the character set \mathcal{C} in order to predict the π_t^{th} character in the input image \mathbf{x} . In particular, our STR model can be formulated by:

$$p_\theta(y_{\pi_t} = c | \mathbf{y}_{\pi_{<t}}, \mathbf{x}) = \sigma(D(E(\mathbf{x}), \pi_t, \mathbf{y}_{\pi_{<t}}))_c \quad (8)$$

where the subscript c is used to indicate the index of the probability vector computed with the softmax function $\sigma(\cdot)$ associated to character c . Furthermore, the parameters $\theta = (\theta_E, \theta_D)$ denote both the encoder and decoder parameter sets, omitted from the Eq. 8 for simplicity.

Permutation Language Decoder (PLD). To enable PLM, the decoder D is implemented with a specific transformer architecture that separates the query stream from the key-value stream, to account for its three inputs (Eq. 8) and to decode the sequence in any order. As shown in Fig. 3, each decoder block is composed by two Multi-Head Cross-Attention layers and by one MLP, with pre-normalization and skip connections. Sequence positions $[1, \dots, L]$ are embedded into positional query vectors $[\mathbf{q}_1, \dots, \mathbf{q}_L]$ that are the input of the query stream: to predict the character in position π_t , positional query \mathbf{q}_{π_t} can be employed. Additionally, positional queries are also used as positional encoding and added to the context, i.e. the embedded sequence of previously predicted characters $\mathbf{y}_{\pi_{<t}}$. Notably, this is introduced as input of the key-value stream in the first Cross-Attention layer, while vision tokens \mathbf{z} are introduced in the second Cross-Attention. Differently from previous approaches [3, 31], when using multiple blocks, we

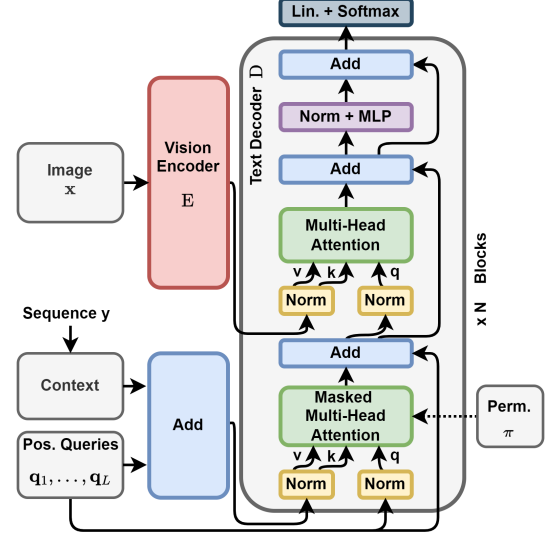


Figure 3. **The overall architecture of our STR model.** Our model mainly consists of **Vision Encoder E** and **Text Decoder D** . Details are given in the Sec. 4.

do not update the context or vision tokens due to observed performance degradation and increased computational complexity as we analyze in the supplementary material (Sec. 7). During training, all the positional queries and the complete ground truth context are utilized to enable parallelism, while the first Cross-Attention is masked to enforce the order of the input permutation π by generalizing the causal mask used in standard language modeling to any permuted order. For more details, refer to [3].

4.1. Scaling Analysis

We analyze how increasing model size can affect the final performance in our STR model, by specifically showing the individual effects of encoder and decoder scaling. To achieve this goal, we consider three image encoders with the same transformer architecture (Vision Transformer [9]) and pre-training scheme (on ImageNet21k [8]), but different parameter capacities: ViT-Tiny, ViT-Small, and ViT-Base. Additionally, we employ Permutation Language Decoders with four different sizes: PLD-Tiny, PLD-Small, PLD-Base, and PLD-Large. The details of these architectures in terms of hyperparameters, number of parameters and GFLOPs are presented in Tab. 1. Additionally, we analyze the effects of training data volume to provide a comprehensive study and novel insights on how to scale STR models effectively in different data volumes.

4.2. Cloze Self-Distillation

Previous empirical evaluations [3, 31] have demonstrated that real datasets offer a better sample-efficiency for training STR models than synthetic datasets, as they are more closely aligned with the target distributions found in STR tasks. However, despite their importance, real datasets of-

		Blocks	Dim	Heads	Params	GFLOPs
ENCODER	ViT-Tiny	12	192	3	5.5 M	2.2
	ViT-Small	12	384	6	21.7 M	8.6
	ViT-Base	12	768	12	85.8 M	33.9
DECODER	PLD-Tiny	1	384	6	2.5 M	0.8
	PLD-Small	1	768	12	9.6 M	3.5
	PLD-Base	2	768	12	19.1 M	7.0
	PLD-Large	3	768	12	28.8 M	12.5
	PLD-Diff	2	768	12	24.4 M	7.1

Table 1. **Details of ViT encoders and PLD decoders** used in our scaling experiments. GFLOPs for the decoder refer to the average test sequence length $L = 5.5$.

ten contain a large number of label errors and inconsistencies, which can adversely impact the performance of STR models, as qualitatively presented in Fig. 2. We propose a novel technique, named **Cloze Self-Distillation (CSD)**, to mitigate the impact of such errors and to improve the STR performance. In particular, CSD is motivated by two key observations:

- After a complete training, the predictions of STR models are, in most cases, more accurate than the actual training labels (see Fig. 2).
- PLM allows to refine the predictions with the cloze-filling approach (end of Sec. 3) and to compute context-aware probabilities for each position t in the sequence given all the other characters $\hat{y}_{\neq t}$ as context.

Given a dataset $\mathcal{S}_{\text{noise}}$ with potential label noise, CSD involves three main steps: **(i)** a teacher STR model p_{θ_T} is fully trained on the noisy dataset $\mathcal{S}_{\text{noise}}$; **(ii)** p_{θ_T} is employed to compute pseudolabels and context aware-logits with the cloze-filling refinement for the dataset $\mathcal{S}_{\text{noise}}$; **(iii)** a new student model p_{θ_S} (with the same architecture and size of the initial model) is distilled from the teacher. Hence, teacher pseudolabels are used instead of the ground truth annotations to minimize the negative log likelihood (NLL) objective of Eq. 6 and an additional Knowledge Distillation (KD) loss term is introduced to minimize the divergence between the context-aware soft predictions of the teacher (obtained with cloze-filling) and the partial-context predictions of the student (obtained with PLM), as it is illustrated in Fig. 4. Formally, the KD term can be formulated by:

$$\text{KD}_{\pi,t}(\mathbf{x}, \mathbf{y}) = D_{\text{KL}}(p_{\theta_T}^{\tau}(\cdot | \mathbf{y}_{\pi_{\neq t}} \mathbf{x}) || p_{\theta_S}^{\tau}(\cdot | \mathbf{y}_{\pi_{< t}} \mathbf{x})) \quad (9)$$

where the superscript τ is used to indicate that the logits of the models are scaled with temperature τ before computing the softmax outputs. We remark that the teacher soft-predictions are computed given the full context, $\mathbf{y}_{\pi_{\neq t}}$, while the student outputs are computed with the standard context of PLM, $\mathbf{y}_{\pi_{< t}}$. This intuitively makes the task more challenging for the student, allowing it to effectively distill the

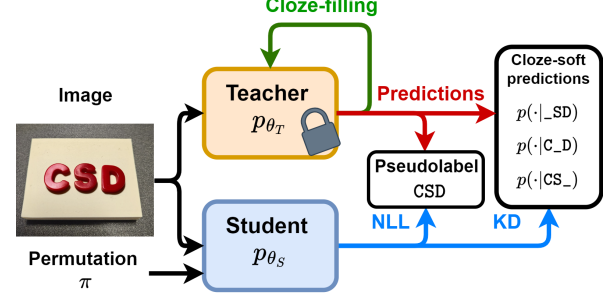


Figure 4. **Flow of Cloze Self-Distillation (CSD)**. Pseudolabels and soft predictions of a fixed teacher model, obtained with the cloze-filling approach, are distilled into a student model by minimizing the negative log likelihood (NLL) and the knowledge distillation (KD) objective, presented in Eq. 10.

knowledge from the teacher and to outperform its performance. The overall CSD objective is:

$$\min_{\theta} \mathbb{E}_{(\mathbf{x}, \mathbf{y}) \sim \mathcal{D}} [-\log p_{\theta}(\mathbf{y}_{\pi_t} | \mathbf{y}_{\pi_{< t}}, \mathbf{x}) + \alpha \text{KD}_{\pi,t}(\mathbf{x}, \mathbf{y})] \quad (10)$$

where the expectation $\mathbb{E}[\cdot]$ is with respect to the data samples (\mathbf{x}, \mathbf{y}) , the permutations π and the position t in the sequence. Furthermore, α is the hyperparameter to define the contribution of distillation term to the objective function.

4.3. Differential Decoder

For the decoder D , we introduce a Differential Cross-Attention mechanism, inspired from the Differential Self-Attention proposed by [50] for NLP. Intuitively, Differential Cross-Attention computes two separate softmax cross-attention maps and subtracts them to cancel out common-noise mode [50]. This enables the Cross-Attention mechanism to focus more on relevant context and vision tokens than noisy-representations (visual examples are presented in the supplementary material, Sec. 10). Formally, let d be the inner dimension of the transformer, h be the number of heads, such that $d_h = \frac{d}{h} \in \mathbb{N}$ is the dimension of each head. Given an input sequence of L_q tokens for the query stream \mathbf{s}_q and an input sequence of L_{kv} tokens for the key-value stream \mathbf{s}_{kv} , for the attention head $i \in [1, \dots, h]$, the differential cross-attention operation is formulated by:

$$\text{Cross-Att}_{\text{DIFF}}^i(\mathbf{s}_q, \mathbf{s}_{kv}) = \left(\sigma \left(\frac{\mathbf{q}_1 \mathbf{k}_1^T}{\sqrt{d}} \right) - \lambda \sigma \left(\frac{\mathbf{q}_2 \mathbf{k}_2^T}{\sqrt{d}} \right) \right) \mathbf{v} \quad (11)$$

where the queries, keys and values in the attention operation can be represented as $\mathbf{q} = [\mathbf{q}_1, \mathbf{q}_2] = \mathbf{s}_q W_i^q$, $\mathbf{k} = [\mathbf{k}_1, \mathbf{k}_2] = \mathbf{s}_{kv} W_i^k$, and $\mathbf{v} = \mathbf{s}_{kv} W_i^v$, where i indicates the head index and W_i^q, W_i^k, W_i^v are the projection matrices and $[\cdot, \cdot]$ indicates a concatenation operation. λ is a scalar

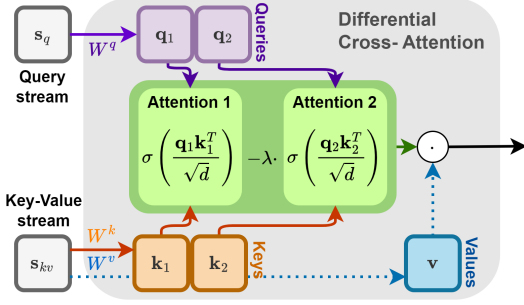


Figure 5. **Differential Cross-Attention** used in our PLD decoder. For simplicity, the diagram shows a single head.

parameter shared across heads of the same layer, that is reparametrized by following [50]. The outputs of the heads are separately normalized using RMSNorm, concatenated and multiplied with an output projection matrix W^o . In our Differential Decoder, we replace all traditional Multi-Head Cross-Attention layers with Multi-Head Differential Cross-Attention layers and utilize MLP with SwiGLU [33]. Differently from [50] RoPE [41] is not applied. A diagram of the Differential Cross-Attention is presented in Fig. 5.

5. Results

5.1. Datasets

In this work, for training, we use a set of Real datasets commonly used in the literature and a superset RBU. For evaluation, we employ 11 test benchmark datasets.

Real Dataset (3.3M images). It is a large scale collection of real datasets including COCO-Text [44], RCTW17 [37], Uber-Text [53], ArT [6], LSVT [42], MLT19 [26], TextOCR [39], ReCTR [52] and OpenVINO [19]. These datasets have samples that cover challenging cases for low-resolution, occluded, curved and rotated text. The detail analysis of these datasets is presented in [15].

RBU (6.5M images). It is the combination of Real dataset (R), the training split of benchmark datasets (B) and a subset of Union14M-L (U). The Benchmark split includes IIIT5K [25], Street View Text (SVT) [45], ICDAR13 [17] and ICDAR15 [18], while the U split includes a subset of approximately 3.5M images from Union14-L [15].

Test Benchmarks. We evaluate STR models on the 6 most widely used benchmarks in the literature: ICDAR13 (IC13) [17], IIIT5K [25], and Street View Text (SVT) [45] for *Regular Text* recognition; and CUTE80 (C80) [32], ICDAR15 (IC15) [18] and Street View Text-Perspective (SVT-P) [28] for *Irregular Text* recognition. The IC13 benchmark includes subsets of 857 images (IC13-857) and a subset of 1015 images (IC13-1015), while IC15 include subsets of 1811 images (IC15-1811) and 2077 images (IC15-2077). Additionally, we report performance on two datasets designed to evaluate robustness for occlusions: Heavily Occluded Scene Text (HOST) and Weakly Occluded Scene Text (WOST) [47]. To further ensure comprehensive evaluation,

we also include more recent and larger benchmarks, COCO-Text [44], ArT [6] and Uber-Text [53].

5.2. Experiment Settings

Pre-processing. For training, input images are augmented using RandAugment [7] using 3 different layers with magnitude 5. By following [3], Sharpness augmentation is excluded, while GaussianBlur and PoissonNoise are added. Images are then resized to 224×224 and their pixel values are normalized to the interval $[-1, 1]$. Since our vision encoder E is based on ViT, images are converted into patches of size 16×16 pixels. Following previous works and to provide comparable results, we set the maximum sequence length L to 25 and we consider a set \mathcal{C} of 94 characters during training (mixed-case alphanumeric and punctuation marks) and a set of 36 characters (lowercase alphanumeric) during test.

Training protocol. Model parameters are optimized with a global batch size of 1024 using AdamW [24] with $\beta_1 = 0.9$, $\beta_2 = 0.95$, 0.1 weight decay and gradients are clipped to 1.0. The learning rate follows a One-Cycle [40] schedule with a maximum value of 0.01 and 3300 warm-up steps, both for encoder and decoder parameters. We train each STR model for 110K steps, corresponding to approximately 35 epochs for Real (R) dataset, 17.5 for RBU. To train the model with Permutation Language Modeling, we follow [3] and employ the causal and anti-causal permutations (left-to-right and right-to-left), together with 4 random permutations sampled differently for each batch. For CSD, the same training schedule is employed both for the teacher and the student and we use $\alpha = 0.1$ and $\tau = 2.0$.

Evaluation metrics. Following previous works, we evaluate our STR model using the *word accuracy*, where a predicted sequence is considered correct only if all characters match the ones of the ground truth label. To make a comparison with the results reported by previous works [31, 54], we provide two separate aggregate scores: the average accuracy across all 11 benchmarks, considering the subsets IC13-1015 and IC15-1811 (it is referred as **AVG₁₁**) and the weighted average of the 6 common benchmarks with the subsets IC13-857 and IC15-1811 (it is referred as **wAVG₆**).

5.3. Encoder-Decoder Scaling results

In this section, we analyze the impact of scaling both the vision encoder and the text decoder in our STR model. In Tab. 2, we present the average word accuracy **AVG₁₁** achieved with various encoder and decoder configurations (introduced in Sec. 4.1). Furthermore, Fig. 1 provides a visual comparison of these results, highlighting how proper model scaling can outperform the previous state-of-the-art (CLIP4STR [54]) using significantly less parameters.

Encoder scaling. From the results, scaling the vision encoder from ViT-T to ViT-S significantly boosts the accuracy

	Dataset	PLD-T	PLD-S	PLD-B	PLD-L
ViT-T	Real	90.08	91.06	91.63	91.67
	RBU	90.15	91.13	91.86	91.93
ViT-S	Real	91.04	91.67	92.21	92.36
	RBU	91.28	92.24	92.62	92.77
ViT-B	Real	90.81	91.41	91.97	92.52
	RBU	91.55	92.38	92.78	92.98

Table 2. **Encoder-Decoder Scaling.** Average word accuracy (%) on the 11 benchmarks (AVG_{11}) for different encoder-decoder configurations trained on Real or RBU dataset.

	ViT-T			ViT-S			ViT-B		
P	✗	✓	✓	✗	✓	✓	✗	✓	✓
KD	✗	✗	✓	✗	✗	✓	✗	✗	✓
AVG_{11}	91.6	91.8	91.9	92.2	92.4	92.5	92.0	92.3	92.5

Table 3. **Effects of pseudolabels and KD.** Average word accuracy (%) on 11 benchmarks (AVG_{11}) using the Real dataset with standard supervised training, pseudolabels (P) and Knowledge Distillation (KD) with the cloze soft probabilities. Results are shown for different encoders paired with the base decoder (PLD-B).

	Real				RBU
	10%	25%	50%	100%	200%
Sup.	86.9	89.9	90.8	92.0	92.8
CSD	89.1	91.1	91.7	92.5	93.2

Table 4. **Benefits of CSD.** Average word accuracy (%) on the 11 benchmarks (AVG_{11}) of ViT-B and PLD-B scaling the data samples from 0.33M (10%) to 6.5M (200%). Standard supervised training (Sup.) is compared to our approach (CSD).

Decoder	Params	GFLOPs	Real		RBU	
			AVG_{11}	wAVG_6	AVG_{11}	wAVG_6
PLD-B	104.9 M	40.9	92.5	97.3	93.2	97.5
PLD-D	110.2 M	41.0	92.7	97.4	93.3	97.6

Table 5. **Benefits of Differential Decoder (PLD-D).** AVG_{11} and wAVG_6 of ViT-B paired with the standard base decoder (PLD-B) and the differential decoder (PLD-D), trained on Real or RBU dataset. Parameters and GFLOPs refer to the full encoder-decoder architecture, considering the average test sequence length of 5.5.

across both Real and RBU datasets, and for all decoder configurations. However, further scaling from ViT-S to ViT-B, shows a different effect: when data is abundant (on RBU), the larger encoder improves performance with all decoders, but on the Real dataset with smaller decoders, ViT-B decreases the performance compared to ViT-S. Part of this behavior can be explained due to the label noise sensitivity of ViT-B (when paired with a small decoder). In Subsection 5.4, we will show that the impact of label noise can be mitigated by our CSD technique.

Permutation Language Decoder scaling. Our results demonstrate that scaling the decoder is more parameter

(Fig. 1) and computational (Sec. 8) efficient than scaling the encoder only, leading to more favorable scaling laws than previous state-of-the-art approaches. Using the larger RBU dataset as a reference, increasing the encoder from ViT-T to ViT-B yields an average improvement (across decoders) of 1.16% AVG_{11} with an additional 80.3M parameters. In contrast, scaling the decoder from PLD-T to PLD-L results in an average improvement (across encoders) of 1.56% AVG_{11} with only 26.3M parameter increase. Furthermore, on RBU, ViT-B paired with PLD-L (114.6M total parameters) obtains an average accuracy AVG_{11} of 92.98% surpassing the 92.80% accuracy of CLIP4STR-H (1B parameters). Similar trends can be observed also on the Real dataset, where ViT-T, ViT-S and ViT-B configurations achieve notable performance gains when the decoder size is increases, and, the transition from PLD-T to PLD-L provides +1.59%, +1.32% and +1.71%, respectively.

5.4. Cloze Self-Distillation results

Table 3 presents the average word accuracy (AVG_{11}) obtained with different training procedures: standard supervised training, training on teacher pseudolabels (P) and CSD (pseudolabels and Knowledge Distillation (KD)). In this experiment, we utilize ViT of varying sizes (Tiny, Small, Base) as encoders, paired with the base-size decoder (PLD-B). Notably, incorporating teacher pseudolabels during training significantly enhances the performance, since it reduces the label errors and inconsistencies in real datasets. Moreover, integrating the Knowledge Distillation component based on context-aware probabilities (computed with the cloze-filling approach) further strengthens the regularization effects, resulting in an additional performance gain. The superiority of CSD is evident also in Table 4, which reports the average accuracy of ViT-Base with PLD-B when scaling the data from 10% to 100% of the Real dataset, as well as on RBU (which represents approximately 200% of the Real dataset). Compared to the baseline method of standard supervised training, CSD consistently provides notable improvements at all data scales. Our technique achieves $\sim 0.5\%$ accuracy gain both when the full Real dataset or RBU dataset are used (for comparison, doubling the training dataset, i.e., Real \rightarrow RBU, yields a +0.8% performance increase). This demonstrates the effectiveness of CSD at any data scale. Additional considerations about the effectiveness of CSD are presented in the supp. material (Sec. 11).

5.5. Differential decoder

To enhance the performance of CSD without a significant increase in GFLOPs, we introduce the differential decoder PLD-Diff (Sec. 4.3). We evaluate its effectiveness in the base configuration with 2 layers, an inner dimension of 768 and 12 attention heads and with ViT-Base encoder (Tab. 1). Tab. 5 shows that PLD-Diff consistently improves the per-

Method	Data	Params	Regular text				Irregular Text				Occluded Text		Other			AVG ₁₁
			IC13		IIIT5k	SVT	C80	IC15	SVTP	HOST	WOST	ArT	COCO	Uber		
			857	1015	3000	647	288	1811	2077	645	2416	2416	34k	9825	89.5k	
VITSTR-S [1]	Real	21.7 M	97.6	97.7	98.1	95.8	96.1	88.4	87.1	91.4	64.5 [*]	77.9 [*]	81.1	74.1	78.2	85.8
CRNN [35]	Real	8.5 M	94.1	94.5	94.6	90.7	89.1	82.0	78.5	80.6	-	-	66.8	62.2	51.0	-
TRBA [2]	Real	49.6 M	97.6	97.6	98.6	97.0	97.7	89.8	88.7	93.7	-	-	82.5	77.5	81.2	-
ABINET [10]	Real	23.5 M	98.0	97.8	98.6	97.8	97.7	90.2	88.5	93.9	72.2 [*]	85.0 [*]	81.2	76.4	71.5	87.5
PARSeq [3]	Real	22.5 M	98.3	98.4	99.1	97.9	98.3	90.7	89.6	95.7	74.4 [*]	85.4 [*]	84.5	79.8	84.5	89.9
CLIP4STR-B [54]	Real	158 M	98.4 [†]	98.3	99.2	98.3	99.3	91.4	90.6	97.2	77.5	87.5	85.8	81.1	86.8	91.1
CLIP4STR-L [54]	Real	446 M	98.5 [†]	<u>98.5</u>	99.5	<u>98.5</u>	<u>99.0</u>	91.3	90.8	97.4	79.8	89.2	85.9	81.9	87.6	91.7
CSD-S (ours)	Real	40.8 M	<u>99.1</u>	98.8	<u>99.4</u>	<u>98.5</u>	<u>99.0</u>	91.9	91.3	97.5	<u>83.5</u>	90.9	86.2	<u>82.7</u>	89.6	<u>92.5</u>
CSD-B (ours)	Real	104.9 M	99.2	98.8	<u>99.4</u>	98.0	<u>99.0</u>	92.5	<u>91.6</u>	<u>97.8</u>	83.6	90.0	86.2	82.8	<u>89.7</u>	<u>92.5</u>
CSD-D (ours)	Real	110.2 M	99.0	98.8	99.3	99.1	99.3	<u>92.4</u>	91.7	98.1	83.6	<u>90.8</u>	<u>86.1</u>	82.6	89.8	92.7
CLIP4STR-B [54]	RBU	158 M	-	98.6	<u>99.5</u>	98.3	99.0	91.4	91.1	98.0	79.3	88.8	85.8	81.3	92.1	92.0
CLIP4STR-L [54]	RBU	446 M	-	<u>99.0</u>	99.6	98.6	99.7	91.9	91.4	<u>98.1</u>	81.1	90.6	86.4	82.7	92.2	92.7
CLIP4STR-H [54]	RBU	1 B	-	98.9	<u>99.5</u>	<u>99.1</u>	99.0	91.7	91.0	98.0	82.6	<u>90.9</u>	86.4	83.0	91.7	92.8
CSD-S (ours)	RBU	40.8 M	98.7	98.6	99.2	98.8	99.0	92.2	91.7	97.8	84.3	89.5	<u>86.3</u>	82.9	91.7	92.8
CSD-B (ours)	RBU	104.9 M	<u>98.8</u>	98.7	<u>99.5</u>	98.8	99.3	<u>92.6</u>	92.2	98.3	84.2	91.2	86.4	83.4	<u>93.1</u>	<u>93.2</u>
CSD-D (ours)	RBU	110.2 M	99.2	99.2	<u>99.5</u>	99.2	99.7	92.7	<u>91.9</u>	<u>98.1</u>	84.3	90.6	86.4	<u>83.1</u>	93.2	93.3

Table 6. **Comparison with state-of-the-art methods.** The word accuracy (%) of our models trained with CSD is compared with state-of-the-art approaches both for the Real and RBU training datasets. Results marked with * are from [54], results marked with [†] are from [31]. The best results are highlighted in **bold**, while second-best results are underlined.

formance using both Real and RBU datasets. As claimed in [50], in a traditional Cross-Attention mechanism, a small proportion of attention maps might focus on relevant context. Hence, this leads to poor predictions and decreases the performance. In contrast, Differential attention concentrates more on critical information, so that a performance increase can be observed. Furthermore, PLD-Diff adds 5.7M parameters (compared to PLD-Base), but only 0.1 GFLOPs by considering an average sequence length of 5.5.

5.6. Comparison with State-of-the-Art

We compare our CSD technique and differential decoder with previous approaches. Specifically, we focus on three different model configurations:

- **CSD-S** (40.8M parameters): ViT-Small + PLD-Base
- **CSD-B** (104.9M parameters): ViT-Base + PLD-Base
- **CSD-D** (110.2M parameters): ViT-Base + PLD-Diff

Table 6 shows that our models outperform previous state-of-the-art models in almost all benchmarks, whether they are trained on the Real or RBU dataset. Precisely, when they are trained solely on the Real dataset, our models outperform the previous state-of-the-art models on 10 out of 11 benchmarks, while requiring significantly less parameters and GFLOPs. Our best model, CSD-D, achieves an **AVG₁₁** accuracy of 92.73% and a **wAVG₆** accuracy of 97.42%, compared to CLIP4STR-L whose respective scores are 91.69% and 97.04%. Note that our models use only 24.7% of the parameters and 23.9% of the GFLOPs achieved by CLIP4STR-L. By expanding the training dataset to RBU, our models continue to outperform previous models, with CSD-D achieving an **AVG₁₁** accuracy of 93.30% and a **wAVG₆** accuracy of 97.62%, even outperforming the 97.42% **wAVG₆** achieved by CLIP4STR-L when scaled to

the larger RBU-Syn dataset whose size is 18M [31].

Even if our method also achieves similar performance compared to DTrOCR [11] in most benchmarks, we have not included their results in this section, since they employ a training set with billions of additional images and the code/weights have not been released.

5.7. Additional analyses

In the supplementary material, we report additional results and ablation studies. In Sec. 8, we provide a detailed analysis of GFLOPs by considering the impact of the decoder with varying sequence lengths. In Sec. 9, we analyze the effect of CSD hyperparameters (i.e., temperature τ and KD loss mixing parameter α). In Sec. 10, 11 and 12 we present additional results and analyses to support the superiority of our model and methodology.

6. Conclusion

In this work, we present a comprehensive analysis of encoder-decoder scaling for STR by demonstrating the significant benefits of scaling the decoder. Additionally, we introduce a novel training strategy to address label noise in real-world STR datasets. We leverage context-aware predictions generated from a teacher model through a cloze-filling approach, to distill a student model with improved performance. Moreover, we propose architectural updates, including Differential Cross-Attention, to improve the effectiveness of the decoder to focus on relevant context during inference. Empirical evaluations show the superiority of our model, achieving SOTA across multiple benchmarks while using fewer parameters and reducing the computational overhead (FLOPs) compared to previous models.

References

- [1] Rowel Atienza. Vision transformer for fast and efficient scene text recognition. In *International conference on document analysis and recognition*, pages 319–334. Springer, 2021. 1, 3, 8
- [2] Jeonghun Baek, Geewook Kim, Junyeop Lee, Sungrae Park, Dongyoon Han, Sangdoo Yun, Seong Joon Oh, and Hwal-suk Lee. What is wrong with scene text recognition model comparisons? dataset and model analysis. In *Proceedings of the IEEE/CVF international conference on computer vision*, pages 4715–4723, 2019. 3, 8
- [3] Darwin Bautista and Rowel Atienza. Scene text recognition with permuted autoregressive sequence models. In *European conference on computer vision*, pages 178–196. Springer, 2022. 2, 3, 4, 6, 8, 1
- [4] Ayan Kumar Bhunia, Aneeshan Sain, Pinaki Nath Chowdhury, and Yi-Zhe Song. Text is text, no matter what: Unifying text recognition using knowledge distillation. In *Proceedings of the IEEE/CVF International Conference on Computer Vision*, pages 983–992, 2021. 3
- [5] Fedor Borisjuk, Albert Gordo, and Viswanath Sivakumar. Rosetta: Large scale system for text detection and recognition in images. In *Proceedings of the 24th ACM SIGKDD international conference on knowledge discovery & data mining*, pages 71–79, 2018. 3
- [6] Chee Kheng Chng, Yuliang Liu, Yipeng Sun, Chun Chet Ng, Canjie Luo, Zihan Ni, ChuanMing Fang, Shuaitao Zhang, Junyu Han, Errui Ding, et al. Icdar2019 robust reading challenge on arbitrary-shaped text-rrc-art. In *2019 International Conference on Document Analysis and Recognition (ICDAR)*, pages 1571–1576. IEEE, 2019. 6
- [7] Ekin D Cubuk, Barret Zoph, Jonathon Shlens, and Quoc V Le. Randaugment: Practical automated data augmentation with a reduced search space. In *Proceedings of the IEEE/CVF conference on computer vision and pattern recognition workshops*, pages 702–703, 2020. 6
- [8] Jia Deng, Wei Dong, Richard Socher, Li-Jia Li, Kai Li, and Li Fei-Fei. Imagenet: A large-scale hierarchical image database. In *2009 IEEE conference on computer vision and pattern recognition*, pages 248–255. Ieee, 2009. 4
- [9] Alexey Dosovitskiy. An image is worth 16x16 words: Transformers for image recognition at scale. *arXiv preprint arXiv:2010.11929*, 2020. 3, 4
- [10] Shancheng Fang, Hongtao Xie, Yuxin Wang, Zhendong Mao, and Yongdong Zhang. Read like humans: Autonomous, bidirectional and iterative language modeling for scene text recognition. In *Proceedings of the IEEE/CVF conference on computer vision and pattern recognition*, pages 7098–7107, 2021. 3, 8
- [11] Masato Fujitake. Dtrocr: Decoder-only transformer for optical character recognition. In *Proceedings of the IEEE/CVF Winter Conference on Applications of Computer Vision*, pages 8025–8035, 2024. 3, 8
- [12] Alex Graves, Santiago Fernández, Faustino Gomez, and Jürgen Schmidhuber. Connectionist temporal classification: labelling unsegmented sequence data with recurrent neural networks. In *Proceedings of the 23rd international conference on Machine learning*, pages 369–376, 2006. 2
- [13] Pan He, Weilin Huang, Yu Qiao, Chen Loy, and Xiaoou Tang. Reading scene text in deep convolutional sequences. In *Proceedings of the AAAI conference on artificial intelligence*, 2016. 2
- [14] Geoffrey Hinton. Distilling the knowledge in a neural network. *arXiv preprint arXiv:1503.02531*, 2015. 2, 3
- [15] Qing Jiang, Jiapeng Wang, Dezhi Peng, Chongyu Liu, and Lianwen Jin. Revisiting scene text recognition: A data perspective. In *Proceedings of the IEEE/CVF international conference on computer vision*, pages 20543–20554, 2023. 1, 6
- [16] Jared Kaplan, Sam McCandlish, Tom Henighan, Tom B Brown, Benjamin Chess, Rewon Child, Scott Gray, Alec Radford, Jeffrey Wu, and Dario Amodei. Scaling laws for neural language models. *arXiv preprint arXiv:2001.08361*, 2020. 2
- [17] Dimosthenis Karatzas, Faisal Shafait, Seiichi Uchida, Masakazu Iwamura, Lluís Gomez i Bigorda, Sergi Robles Mestre, Joan Mas, David Fernandez Mota, Jon Almazan Almazan, and Lluís Pere De Las Heras. Icdar 2013 robust reading competition. In *2013 12th international conference on document analysis and recognition*, pages 1484–1493. IEEE, 2013. 6
- [18] Dimosthenis Karatzas, Lluís Gomez-Bigorda, Angelos Nicolaou, Suman Ghosh, Andrew Bagdanov, Masakazu Iwamura, Jiri Matas, Lukas Neumann, Vijay Ramaseshan Chandrasekhar, Shijian Lu, et al. Icdar 2015 competition on robust reading. In *2015 13th international conference on document analysis and recognition (ICDAR)*, pages 1156–1160. IEEE, 2015. 6
- [19] Ilya Krylov, Sergei Nosov, and Vladislav Sovrasov. Open images v5 text annotation and yet another mask text spotter. In *Asian Conference on Machine Learning*, pages 379–389. PMLR, 2021. 6
- [20] Chen-Yu Lee and Simon Osindero. Recursive recurrent nets with attention modeling for ocr in the wild. In *Proceedings of the IEEE conference on computer vision and pattern recognition*, pages 2231–2239, 2016. 3
- [21] Minghao Li, Tengchao Lv, Jingye Chen, Lei Cui, Yijuan Lu, Dinei Florencio, Cha Zhang, Zhoujun Li, and Furu Wei. Trocr: Transformer-based optical character recognition with pre-trained models. In *Proceedings of the AAAI Conference on Artificial Intelligence*, pages 13094–13102, 2023. 3
- [22] Wei Liu, Chaofeng Chen, Kwan-Yee K Wong, Zhizhong Su, and Junyu Han. Star-net: a spatial attention residue network for scene text recognition. In *BMVC*, page 7, 2016. 2
- [23] Shangbang Long, Xin He, and Cong Yao. Scene text detection and recognition: The deep learning era. *International Journal of Computer Vision*, 129(1):161–184, 2021. 1
- [24] I Loshchilov. Decoupled weight decay regularization. *arXiv preprint arXiv:1711.05101*, 2017. 6
- [25] Anand Mishra, Karteek Alahari, and CV Jawahar. Scene text recognition using higher order language priors. In *BMVC-British machine vision conference*. BMVA, 2012. 6
- [26] Nibal Nayef, Yash Patel, Michal Busta, Pinaki Nath Chowdhury, Dimosthenis Karatzas, Wafa Khelif, Jiri Matas, Uma-

- pada Pal, Jean-Christophe Burie, Cheng-lin Liu, et al. Icdar2019 robust reading challenge on multi-lingual scene text detection and recognition—rrc-mlt-2019. In *2019 International conference on document analysis and recognition (ICDAR)*, pages 1582–1587. IEEE, 2019. 6
- [27] Imene Ouali, Mohamed Ben Halima, and Ali Wali. Text detection and recognition using augmented reality and deep learning. In *International conference on advanced information networking and applications*, pages 13–23. Springer, 2022. 1
- [28] Trung Quy Phan, Palaiahnakote Shivakumara, Shangxuan Tian, and Chew Lim Tan. Recognizing text with perspective distortion in natural scenes. In *Proceedings of the IEEE international conference on computer vision*, pages 569–576, 2013. 6
- [29] Alec Radford, Jeffrey Wu, Rewon Child, David Luan, Dario Amodei, Ilya Sutskever, et al. Language models are unsupervised multitask learners. *OpenAI blog*, 1(8):9, 2019. 3
- [30] Alec Radford, Jong Wook Kim, Chris Hallacy, Aditya Ramesh, Gabriel Goh, Sandhini Agarwal, Girish Sastry, Amanda Askell, Pamela Mishkin, Jack Clark, et al. Learning transferable visual models from natural language supervision. In *International conference on machine learning*, pages 8748–8763. PMLR, 2021. 2
- [31] Miao Rang, Zhenni Bi, Chuanjian Liu, Yunhe Wang, and Kai Han. Large ocr model: An empirical study of scaling law for ocr. *arXiv preprint arXiv:2401.00028*, 2023. 1, 2, 3, 4, 6, 8, 9
- [32] Anhar Risnumawan, Palaiahankote Shivakumara, Chee Seng Chan, and Chew Lim Tan. A robust arbitrary text detection system for natural scene images. *Expert Systems with Applications*, 41(18):8027–8048, 2014. 6
- [33] Noam Shazeer. Glu variants improve transformer. *arXiv preprint arXiv:2002.05202*, 2020. 2, 6
- [34] Fenfen Sheng, Zhineng Chen, and Bo Xu. Nrtr: A no-recurrence sequence-to-sequence model for scene text recognition. In *2019 International conference on document analysis and recognition (ICDAR)*, pages 781–786. IEEE, 2019. 3
- [35] Baoguang Shi, Xiang Bai, and Cong Yao. An end-to-end trainable neural network for image-based sequence recognition and its application to scene text recognition. *IEEE transactions on pattern analysis and machine intelligence*, 39(11):2298–2304, 2016. 2, 8
- [36] Baoguang Shi, Xinggang Wang, Pengyuan Lyu, Cong Yao, and Xiang Bai. Robust scene text recognition with automatic rectification. In *Proceedings of the IEEE conference on computer vision and pattern recognition*, pages 4168–4176, 2016. 3
- [37] Baoguang Shi, Cong Yao, Minghui Liao, Mingkun Yang, Pei Xu, Linyan Cui, Serge Belongie, Shijian Lu, and Xiang Bai. Icdar2017 competition on reading chinese text in the wild (rctw-17). In *2017 14th iapr international conference on document analysis and recognition (ICDAR)*, pages 1429–1434. IEEE, 2017. 6
- [38] Baoguang Shi, Mingkun Yang, Xinggang Wang, Pengyuan Lyu, Cong Yao, and Xiang Bai. Aster: An attentional scene text recognizer with flexible rectification. *IEEE transactions on pattern analysis and machine intelligence*, 41(9):2035–2048, 2018. 3
- [39] Amanpreet Singh, Guan Pang, Mandy Toh, Jing Huang, Wojciech Galuba, and Tal Hassner. Textocr: Towards large-scale end-to-end reasoning for arbitrary-shaped scene text. In *Proceedings of the IEEE/CVF conference on computer vision and pattern recognition*, pages 8802–8812, 2021. 6
- [40] Leslie N Smith and Nicholay Topin. Super-convergence: Very fast training of neural networks using large learning rates. In *Artificial intelligence and machine learning for multi-domain operations applications*, pages 369–386. SPIE, 2019. 6
- [41] Jianlin Su, Murtadha Ahmed, Yu Lu, Shengfeng Pan, Wen Bo, and Yunfeng Liu. Roformer: Enhanced transformer with rotary position embedding. *Neurocomputing*, 568:127063, 2024. 6
- [42] Yipeng Sun, Zihan Ni, Chee-Kheng Chng, Yuliang Liu, Canjie Luo, Chun Chet Ng, Junyu Han, Errui Ding, Jingtuo Liu, Dimosthenis Karatzas, et al. Icdar 2019 competition on large-scale street view text with partial labeling-rrc-lsvt. In *2019 International Conference on Document Analysis and Recognition (ICDAR)*, pages 1557–1562. IEEE, 2019. 6
- [43] Shreyas Vaidya, Arvind Kumar Sharma, Prajwal Gatti, and Anand Mishra. Show me the world in my language: Establishing the first baseline for scene-text to scene-text translation. *arXiv preprint arXiv:2308.03024*, 2023. 1
- [44] Andreas Veit, Tomas Matera, Lukas Neumann, Jiri Matas, and Serge Belongie. Coco-text: Dataset and benchmark for text detection and recognition in natural images. *arXiv preprint arXiv:1601.07140*, 2016. 6
- [45] Kai Wang, Boris Babenko, and Serge Belongie. End-to-end scene text recognition. In *2011 International conference on computer vision*, pages 1457–1464. IEEE, 2011. 6
- [46] Tianwei Wang, Yuanzhi Zhu, Lianwen Jin, Canjie Luo, Xiaoxue Chen, Yaqiang Wu, Qianying Wang, and Mingxiang Cai. Decoupled attention network for text recognition. In *Proceedings of the AAAI conference on artificial intelligence*, pages 12216–12224, 2020. 3
- [47] Yuxin Wang, Hongtao Xie, Shancheng Fang, Jing Wang, Shenggao Zhu, and Yongdong Zhang. From two to one: A new scene text recognizer with visual language modeling network. In *Proceedings of the IEEE/CVF International Conference on Computer Vision*, pages 14194–14203, 2021. 6
- [48] Zixiao Wang, Hongtao Xie, Yuxin Wang, Jianjun Xu, Boqiang Zhang, and Yongdong Zhang. Symmetrical linguistic feature distillation with clip for scene text recognition. In *Proceedings of the 31st ACM International Conference on Multimedia*, pages 509–518, 2023. 3
- [49] Zhilin Yang. Xlnet: Generalized autoregressive pre-training for language understanding. *arXiv preprint arXiv:1906.08237*, 2019. 2, 3
- [50] Tianzhu Ye, Li Dong, Yuqing Xia, Yutao Sun, Yi Zhu, Gao Huang, and Furu Wei. Differential transformer. *arXiv preprint arXiv:2410.05258*, 2024. 2, 5, 6, 8

- [51] Chongsheng Zhang, Weiping Ding, Guowen Peng, Feifei Fu, and Wei Wang. Street view text recognition with deep learning for urban scene understanding in intelligent transportation systems. *IEEE Transactions on Intelligent Transportation Systems*, 22(7):4727–4743, 2020. [1](#)
- [52] Rui Zhang, Yongsheng Zhou, Qianyi Jiang, Qi Song, Nan Li, Kai Zhou, Lei Wang, Dong Wang, Minghui Liao, Mingkun Yang, et al. Icdar 2019 robust reading challenge on reading chinese text on signboard. In *2019 international conference on document analysis and recognition (ICDAR)*, pages 1577–1581. IEEE, 2019. [6](#)
- [53] Ying Zhang, Lionel Gueguen, Ilya Zharkov, Peter Zhang, Keith Seifert, and Ben Kadlec. Uber-text: A large-scale dataset for optical character recognition from street-level imagery. In *SUNw: Scene Understanding Workshop-CVPR*, page 5, 2017. [6](#)
- [54] Shuai Zhao, Ruijie Quan, Linchao Zhu, and Yi Yang. Clip4str: A simple baseline for scene text recognition with pre-trained vision-language model. *arXiv preprint arXiv:2305.14014*, 2023. [1](#), [2](#), [6](#), [8](#), [3](#)

Accurate Scene Text Recognition with Efficient Model Scaling and Cloze Self-Distillation

Supplementary Material

7. Context Update in Permutation Language Decoder

In Sec. 4, we introduced the architecture of the Permutation Language Decoder (PLD) used in our STR model. Specifically, in our implementation, each block of PLD receives the output of the previous block as the input of the query stream, while the key-value stream is provided with the same context and vision tokens across all blocks. It simplifies the original approach used in PARSeq [3], which updates the context when multiple blocks are presented. While the positional queries in PARSeq follow the same query stream as in our implementation, PARSeq additionally provides the context as input to the query stream in a second forward pass. This is done in order to update it before using it as input of the key-value stream of the next block. Fig. 6 shows the diagram of PLD in the PARSeq implementation: the positional queries follow the same path as in our implementation (black arrows), the context is updated following the red arrows.

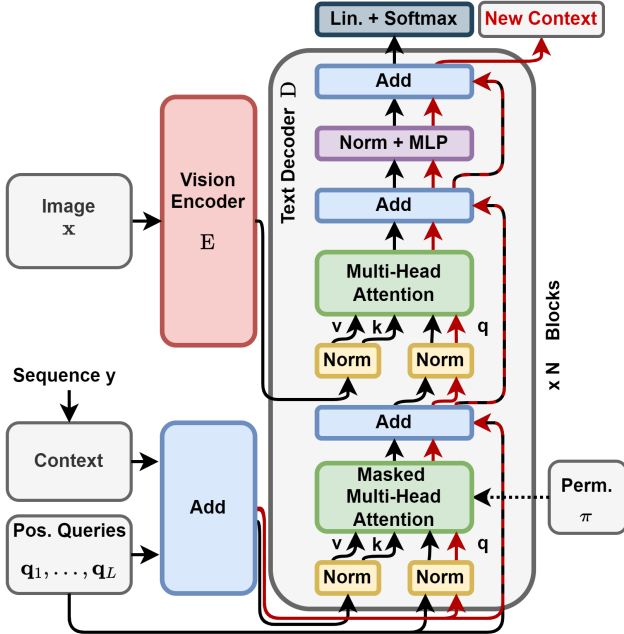


Figure 6. **Diagram of the context update in PLD.** The positional queries are updated following the black arrows (as in our Permutation Language Decoder). The context is updated following the red arrows: it is used as input of the query stream in a second forward pass before using it in the following block.

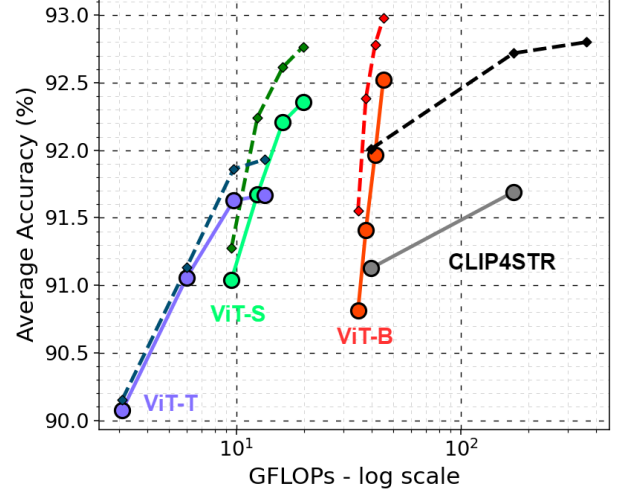


Figure 7. **Average word accuracy (%)** on 11 STR benchmarks for the models with ViT-T, ViT-S and ViT-B vision encoders and 4 different decoder sizes (see Sec. 4.1). Results are compared with the previous state-of-the-art model, CLIP4STR [54]. Results using **Real** training dataset (3.3M images) are depicted with solid lines and circle markers, while results using **RBU** training dataset (6.5M images) are shown with dashed lines and diamond markers. The x-axis represents the **total number GFLOPs** on a logarithmic scale.

Empirically, we found that this additional context update degrades the performance. Considering the average word accuracy across 11 benchmarks (AVG_{11}), the performance of ViT-Base with PLD-Base decreases 0.15%, while ViT-Small and PLD-Base have a decrease of 0.19%. Moreover, since the context is also updated, the computational complexity is also increased. To this end, in all our analyses and experiments, we do not update the context as a default setting.

Remark. In PARSeq paper, they present the results using a single-block decoder so the context is actually not updated. However, their official implementation updates the context when multiple blocks are used.

8. Computational efficiency

In our STR model, the encoder presents a fixed computational cost, as it processes the vision tokens in a single forward pass. In contrast, the computational cost of the decoder depends on the sequence length due to the use of autoregressive (AR) decoding, which has been shown to outperform non-autoregressive (NAR) methods [3]. In Sec. 5.3,

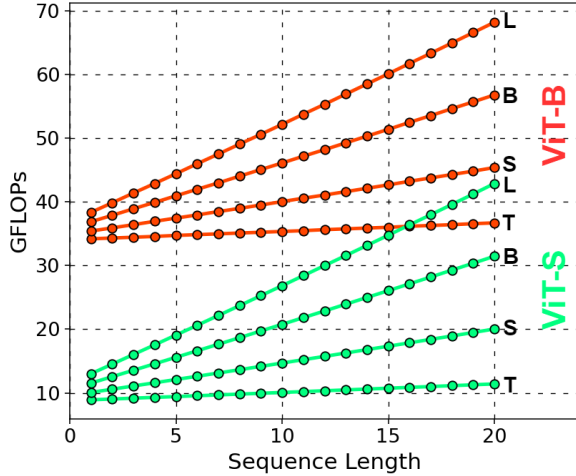


Figure 8. **GFLOPs for different sequence lengths.** The x-axis represents the sequence length (from 1 to 20 characters), while the y-axis represents the number of GFLOPs. Results are reported for ViT-Base and ViT-Small encoders paired with different decoders (PLD-T, PLD-S, PLD-B and PLD-L).

we demonstrated that increasing the decoder size is effective to improve performance. In this section, we analyze the impact of decoder size on overall GFLOPs.

Fig. 7 illustrates how the average model accuracies and the GLOPs change together. A similar plot is provided in Fig. 1 for the average model accuracy and the total number of parameters. The GFLOPs are calculated based on the average sequence length of 5.5, which corresponds to the average sequence length across all benchmark datasets. The plot reveals a similar trend that is observed for the number of parameters. Additionally, Fig. 8 shows how GFLOPs vary across different sequence lengths (from 3 to 20 characters) for various decoder sizes using ViT-B and ViT-S as encoders. Notably, for short sequence lengths, the encoder has the highest computational cost compared to the decoder. However, as the sequence length increases, decoder’s GFLOPs increase, particularly for larger decoders. In most STR tasks, efficiency for long sequences is not a primary target since this kind of sequences is less common in natural scene settings.

Remark. When referring to the sequence length, we specifically consider the number of characters to be decoded. In the actual implementation, two additional special tokens are also decoded: the beginning-of-sequence token (BOS) and the end-of-sequence token (EOS), which mark the start and end of decoding process, respectively. The computation of these tokens is included in the GFLOPs calculation for any sequence length.

9. Cloze Self-Distillation: hyperparameters

In Sec. 4.2, we introduced Cloze Self-Distillation, our novel technique to train STR models on real data. The objective

	$\alpha = 0.1$	$\alpha = 0.5$	$\alpha = 1.0$
$\tau = 1.0$	92.4	92.4	92.5
$\tau = 2.0$	92.5	92.5	92.5
$\tau = 3.0$	92.5	92.6	92.6

Table 7. **CSD hyperparameters.** Average word accuracy (%) AVG_{11} using CSD-B (ViT-Base + PLD-Base) with Real dataset for different values of mixing parameter α and temperature τ .

of CSD is presented in Eq. 10 that we report here for convenience:

$$\min_{\theta} \mathbb{E}_{(\mathbf{x}, \mathbf{y}) \sim \mathcal{D}} [-\log p_{\theta}(y_{\pi_t} | \mathbf{y}_{\pi_{<t}}, \mathbf{x}) + \alpha \text{KD}_{\pi, t}(\mathbf{x}, \mathbf{y})]$$

$\pi \sim \Pi$
 $t \sim [1, L]$

In the experiments presented in the main text, we set the mixing hyperparameter and distillation temperature to $\alpha = 0.1$ and $\tau = 2.0$, respectively. In this section, we present a post-hoc ablation study to show that CSD is not highly sensitive to these hyperparameters. To provide consistent results for different values of α without changing the learning rate and training dynamics, in this section, we multiply the loss by $\frac{1+\alpha_0}{1+\alpha}$, where $\alpha_0 = 0.1$ is our base value for α . Tab. 7 shows that for each combination of α and τ within the considered range, the average word accuracy of CSD surpasses both the accuracy achieved using solely pseudolabels (92.3%) and the accuracy obtained through conventional training methods (92.0%). Moreover, increasing the temperature and mixing parameter appears to further enhance performance beyond the results presented in the main text.

10. Architecture Analysis

In Sec. 4.3, we presented our Permutation Language Decoder equipped with Differential Cross-Attention layers. The aim was to minimize the amount of noise present in the attention maps. Tables 8, 9 and 10 provide visual comparisons between the standard Cross-Attention and our Differential Cross-Attention. From the results, the majority of the noise and errors observed in the standard Cross-Attention are effectively reduced when the Differential Cross-Attention is used.

11. Effectiveness of CSD

All the components of CSD, namely pseudo-labels, knowledge distillation of the context-aware predictions and differential decoder, provide substantial improvements as presented in Tab. 3 and Tab. 4. Specifically, on Real dataset with the base model, pseudo-labels (PL) provide +0.26% improvement by themselves. When PL and context-aware KD are combined, the improvement is +0.50% (providing robustness to label noise). Finally, the differential decoder

(DD) provides an additional relevant improvement (mitigating attention noise): PL + KD + DD obtains +0.70%. Notably, many benchmarks in STR (used to compute the average accuracy) are saturated and affected by test label errors. For this reason, while the improvements might seem modest, they are significant. For comparison, CLIP4STR scales the architecture from 158M to 446M parameters to obtain only +0.56% improvement.

12. Additional Results

In Table 11 and 12, we present qualitative examples of predictions of our STR model by comparing with CLIP4STR [54]. From the results, even if CLIP4STR has a separate branch for text correction, our STR model obtains more accurate results, especially for occluded cases. This shows that training encoder-decoder parts together provides robustness and improves the accuracy. In Table 13 we show that CSD outperforms previous state-of-the-art even in the challenging Union14M benchmark.



Table 8. **Comparison of Attention Maps.** Attention maps of the last Cross-Attention in the last block of the Permutation Language Decoder. On the left: the original input image. First row of each section: attention maps obtained with the standard Cross-Attention. Second row of each section: attention maps obtained with our Differential Cross-Attention.



Table 9. **Comparison of Attention Maps.** Attention maps of the last Cross-Attention in the last block of the Permutation Language Decoder. On the left: the original input image. First row of each section: attention maps obtained with the standard Cross-Attention. Second row of each section: attention maps obtained with our Differential Cross-Attention.



Table 10. **Comparison of Attention Maps.** Attention maps of the last Cross-Attention in the last block of the Permutation Language Decoder. On the left: the original input image. First row of each section: attention maps obtained with the standard Cross-Attention. Second row of each section: attention maps obtained with our Differential Cross-Attention.



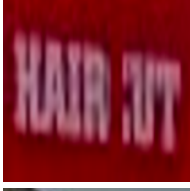


Image	Ground Truth	CLIP4STR-L	CSD-D (ours)	Image	Ground Truth	CLIP4STR-L	CSD-D (ours)
	260	250	260		cheuvront	cheu.ront	cheuvront
	3123410900	3113410900	3123410900		electric	electr.ic	electric
	arlboro	arl.joro	arlioro		cottages	cottages	cottagee
	assistance	wassistance	assistance		cotton	cutton	cutton
	bubble	bubble	bibble		haircut	hai.cut	haircut
	capogiro	cap.giro	capogiro		hotel	lotel	hotel
	centre	centie	centre		kaffee	laffee	kaffee

Table 11. **Qualitative examples.** The table presents image examples along with ground truth labels, predictions made by our models, CSD-D and CLIP4STR-L, which were both trained using the RBU dataset. These predictions are based on a character set consisting of 36 alphanumeric characters. Errors are highlighted in red.








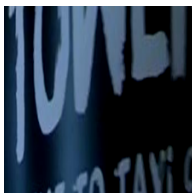
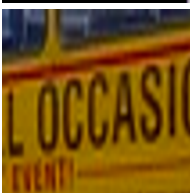
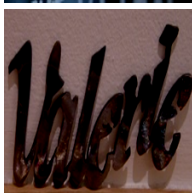

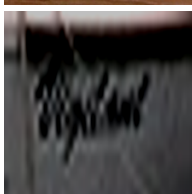
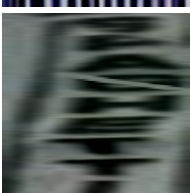

Image	Ground Truth	CLIP4STR-L	CSD-D (ours)	Image	Ground Truth	CLIP4STR-L	CSD-D (ours)
	kennedy	kenned_	kennedy		tabu	tabu	tabu
	lower	power	ower		three	thpee	three
	northeast	northeast	northeast		tigger	tiggen	tigger
	menuboard	menuboard	meruboard		towe_	tower	tower
	loccasio	loccasio	loccasio		valerie	valerte	valerie
	scientific	scientifi_	scentifi_		vigilant	vigitant	vigitant
	spaghetti	spachetti	spaghetti		immortals	immortals	jimmortals

Table 12. **Qualitative examples.** The table presents image examples along with ground truth labels, predictions made by our models, CSD-D and CLIP4STR-L, which were both trained using the RBU dataset. These predictions are based on a character set consisting of 36 alphanumeric characters. Errors are highlighted in red.

Method	Data	Params	Curve	Multi-Oriented	Artistic	Contextless	Salient	Multi-Words	General	Avg
CLIP4STR-B	Real	158M	96.3	96.1	86.5	92.2	91.2	88.9	89.9	91.6
CLIP4STR-L	Real	446M	97.0	96.6	87.2	91.0	91.5	89.9	90.3	91.9
CSD-D (ours)	Real	110M	97.0	97.0	87.7	91.8	91.7	89.5	91.7	92.3
CLIP4STR-B	REBU-Syn	158M	96.4	96.3	88.6	90.1	91.9	92.2	89.1	92.1
CLIP4STR-L	REBU-Syn	446M	96.4	97.2	88.6	90.4	92.7	90.7	89.3	92.2
CSD-D (ours)	RBU	110M	96.5	97.2	88.6	92.8	92.8	90.8	90.2	92.7

Table 13. Comparison of CSD-D with CLIP4STR (results from [31]) on Union14M benchmark.